INTERFACE

rsif.royalsocietypublishing.org

Research

Cite this article: Midgett M, Chivukula VK, Dorn C, Wallace S, Rugonyi S. 2015 Blood flow through the embryonic heart outflow tract during cardiac looping in HH13–HH18 chicken embryos. *J. R. Soc. Interface* **12**: 20150652. http://dx.doi.org/10.1098/rsif.2015.0652

Received: 21 July 2015
Accepted: 21 September 2015

Subject Areas:
biomedical engineering, bioengineering, biomechanics

Keywords:
cardiovascular development, haemodynamics, subject-specific haemodynamic modelling, chick embryo, outflow tract, optical coherence tomography

Author for correspondence:
Sandra Rugonyi
e-mail: rugonyis@ohsu.edu

Electronic supplementary material is available at http://dx.doi.org/10.1098/rsif.2015.0652 or via http://rsif.royalsocietypublishing.org.

THE ROYAL SOCIETY PUBLISHING

Blood flow through the embryonic heart outflow tract during cardiac looping in HH13–HH18 chicken embryos

Madeline Midgett[1], Venkat Keshav Chivukula[1], Calder Dorn[2], Samantha Wallace[2] and Sandra Rugonyi[1]

[1]Department of Biomedical Engineering, Oregon Health and Science University, Portland, OR, USA
[2]School of Chemical, Biological, and Environmental Engineering, Oregon State University, Corvallis, OR, USA

Blood flow is inherently linked to embryonic cardiac development, as haemodynamic forces exerted by flow stimulate mechanotransduction mechanisms that modulate cardiac growth and remodelling. This study evaluated blood flow in the embryonic heart outflow tract (OFT) during normal development at each stage between HH13 and HH18 in chicken embryos, in order to characterize changes in haemodynamic conditions during critical cardiac looping transformations. Two-dimensional optical coherence tomography was used to simultaneously acquire both structural and Doppler flow images, in order to extract blood flow velocity and structural information and estimate haemodynamic measures. From HH13 to HH18, peak blood flow rate increased by 2.4-fold and stroke volume increased by 2.1-fold. Wall shear rate (WSR) and lumen diameter data suggest that changes in blood flow during HH13–HH18 may induce a shear-mediated vasodilation response in the OFT. Embryo-specific four-dimensional computational fluid dynamics modelling at HH13 and HH18 complemented experimental observations and indicated heterogeneous WSR distributions over the OFT. Characterizing changes in haemodynamics during cardiac looping will help us better understand the way normal blood flow impacts proper cardiac development.

1. Introduction

Embryonic cardiac formation is a finely orchestrated interplay between genetic and environmental factors. Blood flow plays a critical role in embryonic heart development, as constant interactions between flow and cardiac tissues generate haemodynamic forces that modulate cardiac growth and remodelling [1–5]. Blood flow exerts pressure and shear stresses on heart walls triggering mechanotransduction mechanisms that lead to physical, chemical and gene regulatory responses in cardiac tissue [6]. Key cardiac morphogenetic events coincide with periods of major haemodynamic change, as the dynamic blood flow environment adjusts to meet the demands of the growing embryo. Normal haemodynamic conditions are essential for proper cardiac development, as several studies have shown that altered blood flow in animal models eventually leads to cardiac defects and malformations [1,3,7–11]. Although it is clear that biomechanical forces are fundamental components of heart morphogenesis, the processes that relate blood flow to cardiac development remain unknown.

This study focuses on characterizing normal changes in blood flow through the outflow tract (OFT) portion of the early embryonic heart. We employed two-dimensional Doppler optical coherence tomography (OCT) to quantify the blood flow environment at each stage during a critical period of cardiac formation from Hamburger and Hamilton (HH) 13 to HH18 in chicken embryos [12]. This developmental period, during which the heart is tubular, includes cardiac looping and the beginning stages of chamber differentiation. The OFT connects the primitive ventricle to the arterial vessel system, is very sensitive to haemodynamic perturbation, and later gives rise to the aorta and pulmonary

trunks, a portion of the interventricular septum, and the semilunar valves, which are often involved in congenital heart defects [3,8,9]. Characterizing the changes in haemodynamics during this period of heart formation will help us better understand the way normal blood flow impacts proper cardiac development and provide a foundation for future studies that investigate how altered haemodynamics lead to cardiac defects.

Blood starts pumping through the embryonic heart at HH10, long before cardiac morphogenesis is complete [13]. Blood pressure is exerted normal to the wall and results from interactions between the wall and blood flow. During myocardial compression, cardiac walls induce an increase in blood pressure. During myocardial relaxation, however, blood pressure generates a tension stress in the heart tissue. Meanwhile, the frictional force of blood flow creates a wall shear stress that acts tangentially to the endocardium [6]. By HH18, endocardial cushions (regional wall thickenings) at the inflow of the OFT function as primitive valves that prevent backflow into the ventricle during diastolic filling [14].

Cardiac looping is an important component of heart morphogenesis. The linear heart tube bends and twists to bring various heart segments into their relative positions to then develop into the four-chambered heart. This process begins soon after beating is initiated and continues through HH16 [14]. Looping is partly mediated by asymmetric gene and molecular expression [15,16], but animal models have also shown that mechanical forces play a major role in the looping process. Various hypotheses of mechanical looping mechanisms have been proposed, where experiments show that several redundant mechanisms are likely involved [17]. These include compressive axial forces as the heart tube lengthens [18], differential growth on either side of the tube [19], active cell shape change [14], cytoskeletal contractions [20] and extrinsic forces from neighbouring tissues [21]. Forces exerted by increasing haemodynamic load during the looping period are likely involved in the structural formation. Abnormal looping can lead to serious structural defects similar to those seen in congenital heart disease. For example, a transient reduction in haemodynamic load after venous obstruction leads to impaired looping [3,22] and subsequent ventricular septal and valve defects [3,9,23,24]. Understanding the dynamic blood flow environments during cardiac looping is essential for defining this important developmental event.

Previous work characterizing cardiac development between HH13 and HH18 has focused on structural changes over the cardiac cycle and stages. External and internal morphological characteristics have been evaluated using cinephotography and videography images to trace embryonic ventricular borders and calculate cardiac volumes [25,26]. Others have defined the diastolic filling characteristics of the embryonic heart, including ventricular pressure, dorsal aortic velocity and atrioventricular blood velocity [27–29]. More recently, four-dimensional OCT has been used in conjunction with computational modelling to analyse the biomechanics through the OFT at HH18 [30,31]. This study focused on haemodynamics in the OFT. We measured OFT blood flow velocity and lumen diameter from Doppler OCT images and calculated peak velocity (*peak V*), peak flow rate (*peak Q*), stroke volume (SV), wall shear rate (WSR), cardiac cycle length and time of flow. Embryo-specific computational fluid dynamics (CFD) simulations were used to complement these measurements and provide additional insights into haemodynamics during the looping stages. This work is the first to report changes in blood flow and WSR through the OFT during cardiac looping from HH13 to HH18.

2. Material and methods

2.1. Chick embryo preparation

Fertilized Brown Leghorn chicken eggs were incubated blunt end up at 37.5°C and 80% humidity until they reached the desired stage. Embryos at stages HH13 (48–52 h of incubation), HH14 (50–53 h), HH15 (50–55 h), HH16 (51–56 h), HH17 (52–64 h) and HH18 (65–69 h) according to the defined Hamburger and Hamilton structural morphology [12] were used in this study ($n = 10$ at each stage). A small section of the blunt-end shell and the inner shell membrane were removed from above the embryo heart. Any embryos that bled upon membrane removal or had obvious structural defects were discarded. Optical microscopy images were then acquired to record developmental stage, using a Leica M165 C Stereomicroscope light microsocpe with PCO-TECH Inc. sCMOS pco.edge 5.5 rolling shutter camera.

2.2. Optical coherence tomography image acquisition

Our custom-made OCT system has been previously detailed and used to image embryonic chicken heart motion and blood flow dynamics [32,33]. Briefly, the system has a spectral domain configuration consisting of a superluminescent diode centred at 1325 nm from Thorlabs Inc. (Newton, NJ, USA) and a 1024 pixel, 92 kHz maximal line-scan rate infrared InGaAs line-scan camera from Goodrich Inc. (Charlotte, NC, USA). This system allowed acquisition of 512 × 512 pixel (512 A-scans) two-dimensional images at approximately 140 frames per second with less than 10 μm resolution. Doppler flow phase images were generated together with simultaneous structural images in post-processing by calculating the phase differences between two adjacent A-scans in a B-scan. Doppler velocities (vertical velocities, V_Z) were then computed from phase data, and the accuracy of these velocities was recently confirmed with a syringe pump [33]. A thermocouple-controlled heating pad surrounding a ceramic cup filled with water was used to maintain temperature in a plastic box during acquisition. This apparatus kept the embryo near 37.5°C in order to maintain the normal physiological heart rate.

For two-dimensional analyses, 200 sequential B-scan frames from a longitudinal plane down the centre of the OFT were acquired for each embryo (approx. three to four cardiac cycles; $n = 10$). The embryo was positioned so that the lumen completely filled the OFT at maximum expansion and made a slit-like shape in the centre of the OFT at maximum contraction [30,34]. A glass capillary tube standard was imaged to calculate a pixel to length conversion factor that was used in all structural analyses. For four-dimensional (three-dimensional over time) analyses, cross-sectional B-scan frames were acquired along the OFT in a representative embryo at HH13 and at HH18. Separation between adjacent cross-sectional planes was 7.5 μm. Following our previously described procedures, these B-scan frame images were synchronized and reconstructed to generate four-dimensional images [35], and the lumen segmented for computational analysis [36].

2.3. Two-dimensional structural and Doppler optical coherence tomography image analyses

Custom Matlab code (The MathWorks, Inc., Natick, MA, USA) was used to extract simultaneous structural and Doppler velocity image datasets from the acquired OCT raw data. A summary of optical, structural OCT and Doppler OCT images acquired at each stage is shown in figure 1. The overall analysis procedure is

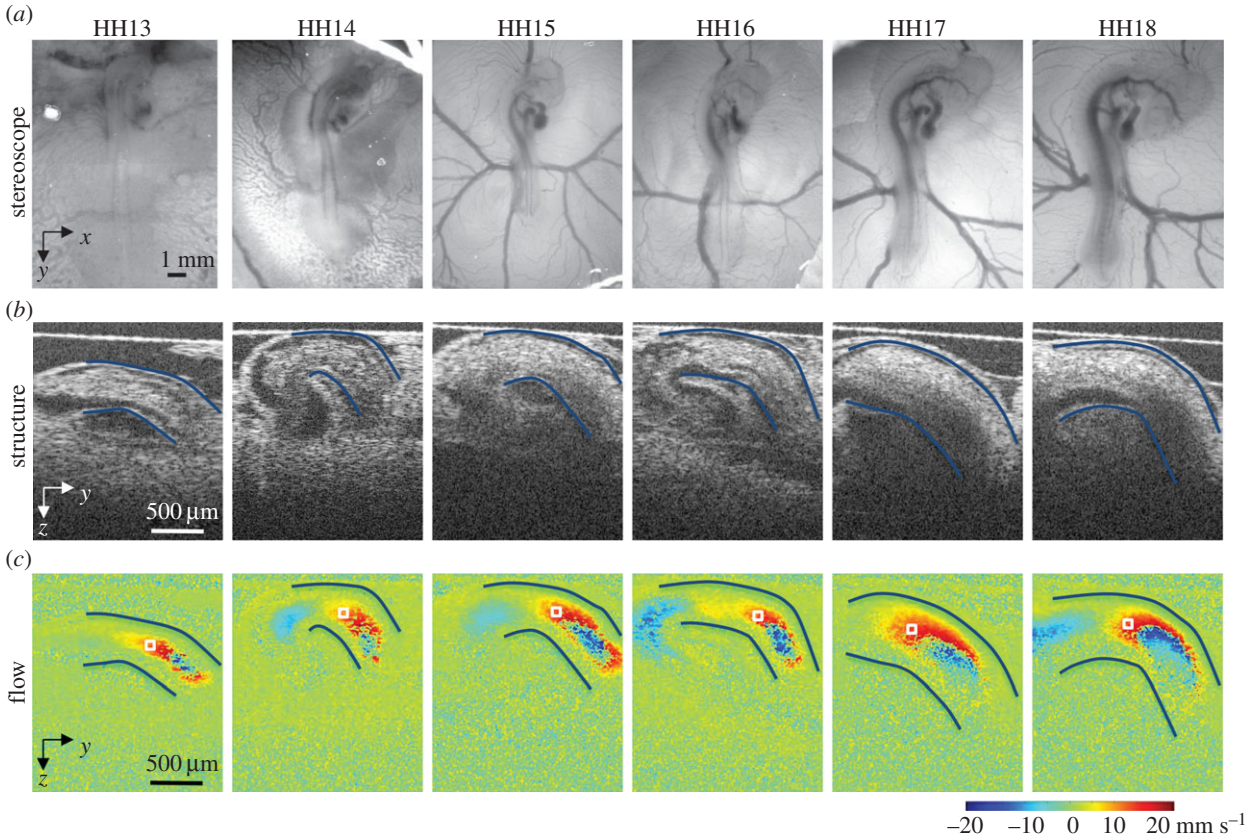

Figure 1. Summary of images acquired from the heart of HH13–HH18 chicken embryos. Example (*a*) shows optical images of the embryo *in ovo* on the top of the egg surface, (*b*) OCT structural two-dimensional longitudinal images of the OFT and neighbouring structures and (*c*) corresponding Doppler OCT images. The OFT myocardial walls are outlined in (*a*,*b*), and the velocity measurement location is marked by a box in (*c*).

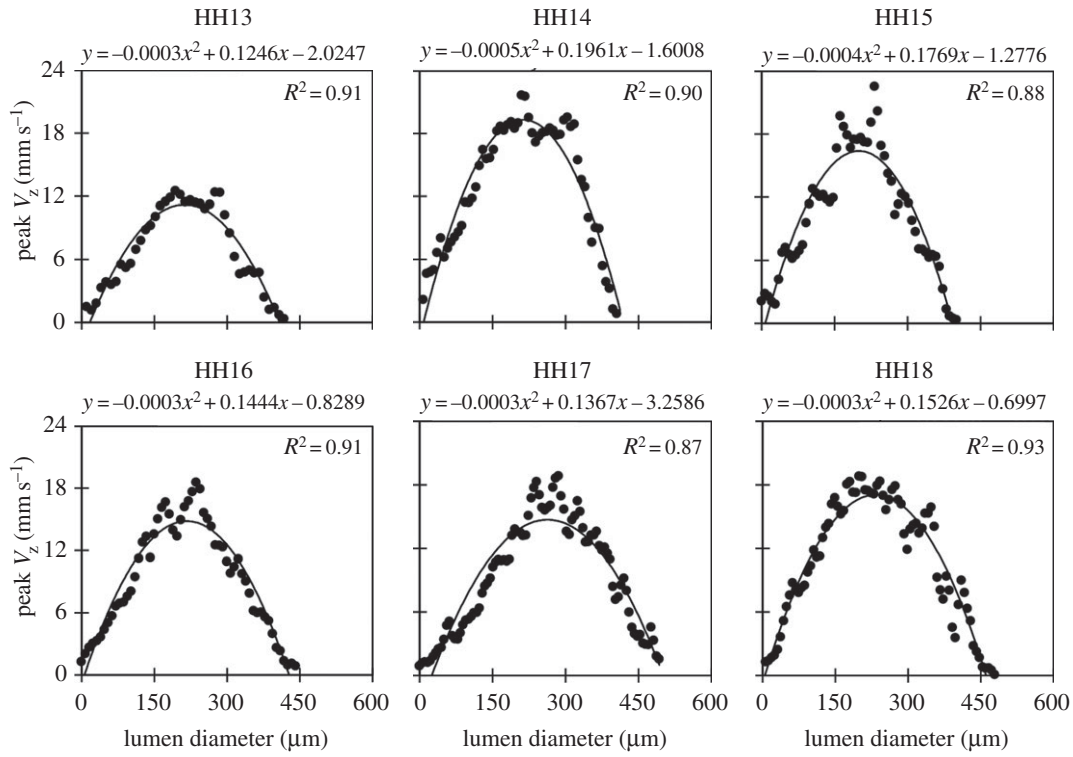

Figure 2. Velocity profiles across the diameter of the OFT during maximum flow for each stage imaged (HH13 to HH18). Vertical velocity (V_Z), depicted for representative embryos at each stage along a line that passes through the sampling point, shows a parabolic-like profile; a second-order polynomial fit and R^2 value are also provided.

very similar to the process we reported for blood flow at HH18 in surgically manipulated and control embryos [33]. This process uses structural data to convert vertical velocity from the Doppler phase data to absolute blood flow velocity magnitude, and then employs Poisseuille's equation to estimate *peak Q*, SV and WSR. Doppler flow combined with structural images show a

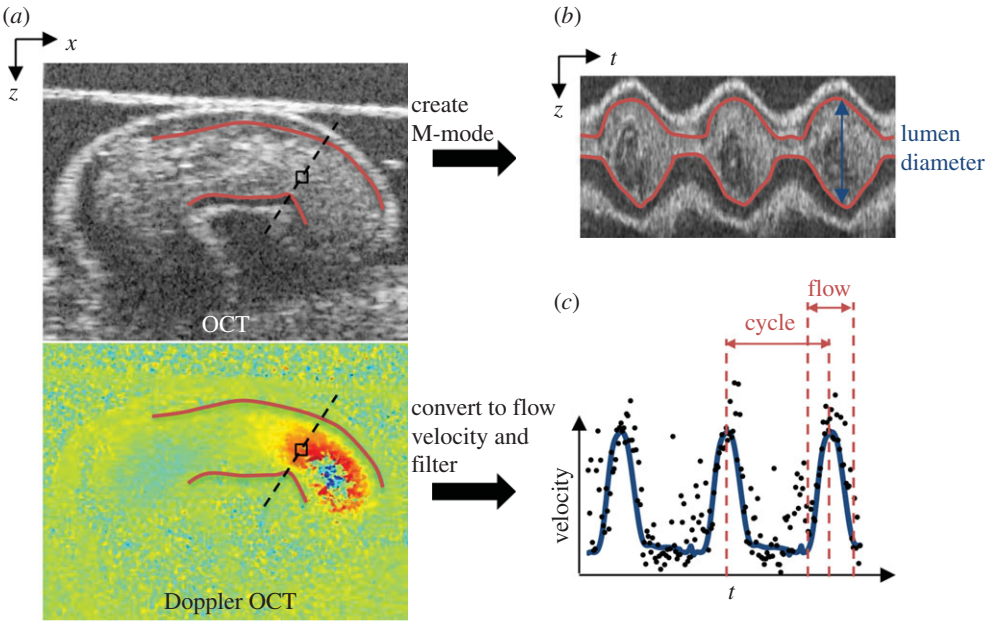

Figure 3. Example HH13 images to summarize image analysis procedure. (*a*) Longitudinal planes through the OFT were imaged with OCT to acquire simultaneous OCT structural and Doppler OCT images. (*b*) M-mode images were created along the dashed line in the OCT structural image in (*a*) over time, from which we calculated lumen diameter (lumen borders are outlined in red). (*c*) Doppler velocity collected from the box in the Doppler OCT image in (*a*) over time, to display velocity over each cardiac cycle (filtered data shown by blue line), and calculate time of flow.

parabolic-like profile of blood flow through the OFT between HH13 and HH18, which make these approximations valid (figure 2). The parabolic profile with low Reynolds ($Re < 4$) and Womersley ($W < 0.6$) numbers, imply that viscous forces dominate blood flow in the OFT. A small Dean number ($De < 3$) implies minor curvature effects in the OFT that cause the blood flow profile to slightly skew towards the inner curvature, especially close to the inlet [37].

Phase wrapping was evident in Doppler images of longitudinal B-scans (figure 1). Wrapping occurs when the phase exceeds $\pm\pi$, which corresponded to vertical velocities higher than $\pm 23.4\ \mathrm{mm\ s^{-1}}$ in our system. Conforming with parabolic-like velocity flow profiles in the OFT from HH13 to HH18 (figure 2) [31,38], the fastest flow often wraps in the centre of the OFT (negative phase enclosed by positive phase), while the slowest/non-wrapped flow develops near the walls. Regions of wrapped and horizontal flow ($V_Z = 0$) in the OFT shifted from HH13 to HH18, as the heart tube underwent looping. Consistent non-wrapped, non-horizontal flow regions along the OFT centreline were identified at each stage and used for the analysis. Regions directly adjacent or within wrapped flow were not chosen for the measurement location to avoid OCT signal deterioration as well as pixel-averaging errors associated with phase wrapping and corresponding unwrapping algorithms. While there were some differences in specific measurement locations across the stages, all velocity sampling areas were selected near the middle region of the OFT. The sampling area used at each stage is shown in figure 1.

Phase shift OCT data within the sampling area were converted to vertical velocity (V_Z) values that were averaged and filtered as previously described [33]. We then calculated the magnitude of the blood flow velocity (V) using:

$$V = \frac{V_z}{\cos\theta}, \tag{2.1}$$

where θ is the angle between the OFT centreline tangent and the vertical direction. Doppler flow and structural images show that blood flow follows the contour of the OFT between HH13 and HH18, so that θ is a good approximation for the angle between V_Z and the flow direction. For each sampling location, θ was measured with a custom Matlab program that calculated the centreline of the OFT during maximum flow by finding the midpoint between outlined upper and lower myocardium walls from longitudinal structural images at each position along the tube. The sampling location was chosen along the OFT centreline, where maximum velocities occurred, and the average *peak V* was calculated as the maximum absolute velocity at the sampling location over the cardiac cycle. This velocity was compared across all stages.

OFT lumen diameters were measured from M-mode image analysis. M-mode images were generated from a line perpendicular to the OFT centreline at the velocity measurement location and used to display grey-scale structure from the chosen line over time (figure 3). The upper and lower lumen interfaces in each M-mode were traced to calculate the lumen diameter (D) over the entire cardiac cycle.

The length of the cardiac cycle and time of flow were also measured to further characterize the relationship between blood flow and OFT wall dynamics at each stage. The length of the cardiac cycle was measured as the time between blood flow velocity peaks, and time of flow was defined as the average percentage of time in the cardiac cycle when the main surge of blood was flowing through the measurement location in the OFT. The presence of flow was determined from the blood flow velocity versus time trace as clear peaks above the background noise level (figure 3).

Volumetric flow rate over time was calculated using a form of the Poiseuille equation [39,40]:

$$Q = \frac{\pi D^2 v_c}{8}, \tag{2.2}$$

where Q is the blood flow rate through the OFT, v_c is the measured OFT centreline velocity (absolute value) and D is the OFT lumen diameter from each frame. Equation (2.2) assumes that blood is homogeneous, with parabolic, fully developed and laminar flow, and zero velocity at the OFT lumen wall. SV was then estimated by summing the forward flowing volume of blood calculated from each frame during flow in a full cardiac cycle:

$$SV = \sum_{i=1}^{N} Q_i \Delta t, \tag{2.3}$$

where $\Delta t = 1/\text{frame rate}$ (140 fps for our system) and N is the number of frames in one cardiac cycle with forward flowing

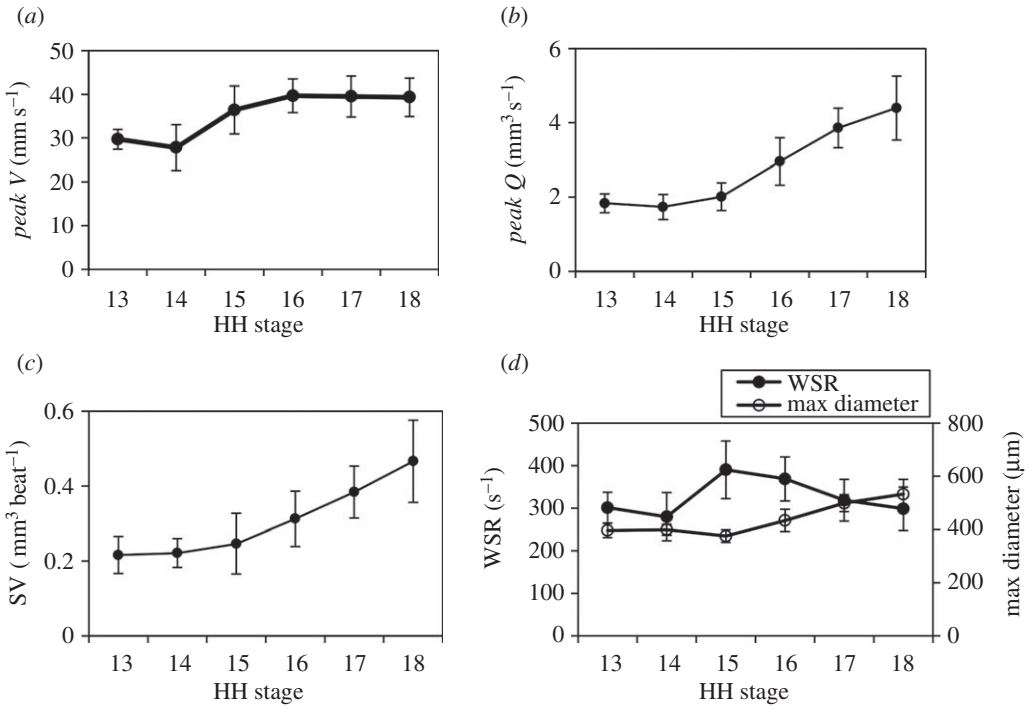

Figure 4. Summary of haemodynamic results over advanced developmental stages from HH13 to HH18 ($n = 10$ at each stage). (*a*) *Peak V* (mm s^{-1}), (*b*) *peak Q* (mm^3 s^{-1}), (*c*) SV (mm^3 $beat^{-1}$) and (*d*) WSR (s^{-1}) with maximum diameter (μm) displayed on the secondary *y*-axis. Average measures are shown at each stage with s.d.

blood (25–45 frames, depending on the cardiac cycle period and time of flow at each stage).

WSR was calculated using another derivation of the Poisseuille equation [41,42]:

$$\mathrm{WSR} = \frac{4v_c}{D}. \tag{2.4}$$

Embryonic chick blood has a fairly constant viscosity in the physiological shear rate range [43], so that WSR should be proportional to wall shear stress. Al-Roubaie *et al*. reported small changes in viscosity during later development over large periods of developmental time (4 days) [44], indicating that the changes in viscosity between HH13 and HH18 (20 h) are likely minimal and can be assumed constant. The WSR at the time of *peak V* in the cardiac cycle was compared across all developmental stages.

2.4. Embryo-specific four-dimensional computational fluid dynamics modelling of haemodynamics in the outflow tract

To complement experimental measurements and to determine three-dimensional distributions of flow and WSR over time, CFD models of the beating heart OFT at HH13 and HH18 were generated. We used four-dimensional embryo-specific geometries of the OFT lumen (segmented from OCT images), which consisted of a sequence of meshes that depicted the dynamic motion of the OFT walls over the cardiac cycle. Blood was modelled as a Newtonian fluid having density $\rho = 1060\ \mathrm{kg\ m^{-3}}$ [43] and viscosity $\mu = 0.003$ Pa s. Embryo-specific blood flow through the OFT was modelled using a recently developed inverse method based optimization procedure [45]. Briefly, normal tractions (pressures) at the OFT lumen inlet and outlet surfaces (or more practically their difference) were iteratively imposed, until computed and measured Doppler velocities at an optimization point in the interior of the lumen differed by less than 1%. One representative embryo each at HH13 and HH18 were modelled. CFD simulations were performed using the software ADINA (Watertown, MA, USA). WSR over the OFT lumen surface were obtained and compared to experimentally derived WSR, as described earlier.

3. Results

Blood flow through the OFT was detected in optical and OCT images from HH13 to HH18 (e.g. figure 1). Optical images show that embryo body size, body curvature and the surrounding vitelline vessel network make pronounced changes during this development period. OCT structural and Doppler images focus on the OFT and show the progression of the cardiac looping process. The HH13 OFT is a mostly straight tube near the edge of the embryo body. Consequently, blood flow through the OFT at HH13 was mostly horizontal until it reached the downstream half of the tube. As the development stages advance, the OFT becomes more curved with larger areas of vertical velocities, the interface between the OFT and ventricle becomes more distinct, and the OFT endocardial cushions become more visible. Cardiac looping and continued development and growth of the embryo and heart affected blood flow dynamics. Vertical velocity profiles, measured from a line perpendicular to the direction of flow extending from the velocity measurement location, revealed a parabolic-like profile at each stage (figure 2), validating the use of the Poisseuille calculations to estimate *Q*, SV and WSR.

3.1. Blood flow (*peak V*, *peak Q* and stroke volume)

Peak V, *peak Q*, SV and WSR were measured at each stage between HH13 and HH18 and compared across all stages ($n = 10$ for each stage; figure 4). We report embryo group data as the mean ± s.d. *Peak V* increased between HH13 and HH18 by 1.3-fold from 29.7 ± 2.2 mm s^{-1} to 39.3 ± 4.4 mm s^{-1}, respectively. The largest increase was between HH14 and HH16, and was followed by a plateau region between

Table 1. Summary of average OFT flow parameters for each developmental stage ($n = 10$). Data presented as means ± s.d. Statistical significance was determined with a two-sample Student's *t*-test, reporting two-tail *p*-values, for HH15 and HH18 values compared to HH13 values.

	HH13	HH14	HH15	HH16	HH17	HH18
peak V (mm s^{-1})	29.7 ± 2.2	27.8 ± 5.2	36.4 ± 5.5*	39.7 ± 3.9	39.5 ± 4.7	39.3 ± 4.4*
max diameter (μm)	397 ± 27	399 ± 21	375 ± 24	434 ± 41.9	499 ± 32	533 ± 55*
peak Q (mm^3 s^{-1})	1.8 ± 0.3	1.7 ± 0.3	2.0 ± 0.4	3.0 ± 0.6	3.9 ± 0.5	4.4 ± 0.9*
WSR (s^{-1})	301 ± 36	280 ± 57	390 ± 68*	369 ± 52	319 ± 49	299 ± 51
cardiac cycle (ms)	599 ± 59	554 ± 58	531 ± 39*	462 ± 66	425 ± 33	419 ± 23*
SV (mm^3 $beat^{-1}$)	0.22 ± 0.05	0.22 ± 0.04	0.25 ± 0.08	0.31 ± 0.07	0.38 ± 0.07	0.47 ± 0.11*
time of flow (%)	41.9 ± 4.3	43.0 ± 6.9	41.4 ± 4.7	44.8 ± 6.1	47.0 ± 6.8	53.3 ± 8.4*

*p-value < 0.05.

HH16 and HH18 (table 1 and figure 4*a*). These values correspond to previously published data at various locations in the OFT measured through a combination of scanning microscopic particle image velocimetry, ultrasound and OCT at HH15 [46], HH17 [44,47] and HH18 [30,31,37,48]. Since the θ estimation in this study was based on the outline of the myocardium walls from OCT structural images (instead of standard ultrasound angle measuring procedures where θ is manually set by the operator), angle estimations were likely very consistent.

Similar to the changes in *peak V* with increased developmental stage, average *peak Q* increased between HH13 and HH18 by 2.4-fold from 1.8 ± 0.3 mm^3 s^{-1} to 4.4 ± 0.9 mm^3 s^{-1}, respectively, with the largest increase between HH15 and HH18 ($n = 10$). These values correspond to previously published data at HH18 [30,31,37,48]. Results are summarized in table 1 and figure 4*b*.

Backflow was detected in the downstream portion of the OFT in Doppler OCT images in at least a portion of embryos at stages HH13–HH17. All HH14 embryos ($n = 10$) exhibited backflow, while no embryos at HH18 displayed backflow. Backflow was present immediately prior to the systolic ejection phase. The volume of the backflow in each cardiac cycle was very small compared to the forward flow SV (less than 6%) at each stage. Additionally, an initial forward flow surge was detected prior to the main ventricle ejection in 50% of HH17 embryos and 100% of HH18 embryos (table 2 and figure 5).

Average SV increased between HH13 and HH18 by 2.1-fold from 0.22 ± 0.05 mm^3 $beat^{-1}$ to 0.47 ± 0.11 mm^3 $beat^{-1}$. These values are comparable to previously published data that was estimated with prolate spheroid ventricular volumes [25]. Results are summarized in table 1 and figure 4*c*.

WSR at peak blood flow velocity at the sampling location in the OFT was calculated at each developmental stage HH13–HH18 ($n = 10$). The average maximum WSR across HH13–HH18 embryos was 301 ± 36 s^{-1} and 299 ± 51 s^{-1}, respectively, which is within previously published experimental and CFD model estimates in the chick embryo OFT at HH17 [47] and HH18 [30]. While there is no net change in WSR from HH13 to HH18, WSR increased between these stages to return to HH13 levels by HH18. WSR peaked at HH15 at 390 ± 68 s^{-1}, which was associated with an increase in *peak V*. OFT lumen diameter remained relatively constant between HH13 and HH15, but then also increased between HH15 and HH18. Results are summarized in table 1 and figure 4*d*.

Table 2. Summary of backflow and forward surge flow presence in embryos at each stage ($n = 10$).

stage	embryos with backflow (%)	embryos with forward surge (%)
HH13	60	0
HH14	100	0
HH15	90	0
HH16	50	0
HH17	40	50
HH18	0	100

3.2. Cardiac cycle (cardiac cycle length and time of flow)

Cardiac cycle length and time of flow were measured at each stage (HH13–HH18) to compare cycle timing ($n = 10$) (figure 6). The cardiac cycle decreased in length with advanced developmental stage between HH13 and HH18 from 599 ± 59 ms to 419 ± 23 ms, respectively. The results are summarized in table 1 and figure 6*a*. Cardiac cycle measured in this study corresponds to previously reported values measured from the dorsal aorta, with increased heart rate with advancing developmental stage [27–29].

The time of flow was measured for all embryos from clearly distinguishable periods of blood flow in the velocity versus time trace from each developmental stage between HH13 and HH18 ($n = 10$). Time of flow, the percentage of time in the cardiac cycle when blood was flowing (main surge), was approximately half of the cardiac cycle for all embryos, consistent with our previous observations at HH18 [30]. The time of flow stayed near constant over the analysed developmental stages and increased slightly between HH13 and HH18 from 41.9 ± 4.3% to 53.3 ± 8.4%, respectively. The results are summarized in table 1 and figure 6*b*.

3.3. Computational fluid dynamics modelling of blood flow in the outflow tract

Four-dimensional embryo-specific CFD modelling of blood flow in the OFT revealed the changes in three-dimensional flow profiles between HH13 and HH18 (figure 7*a*,*b*, top rows). Velocity profiles were skewed towards regions of inner

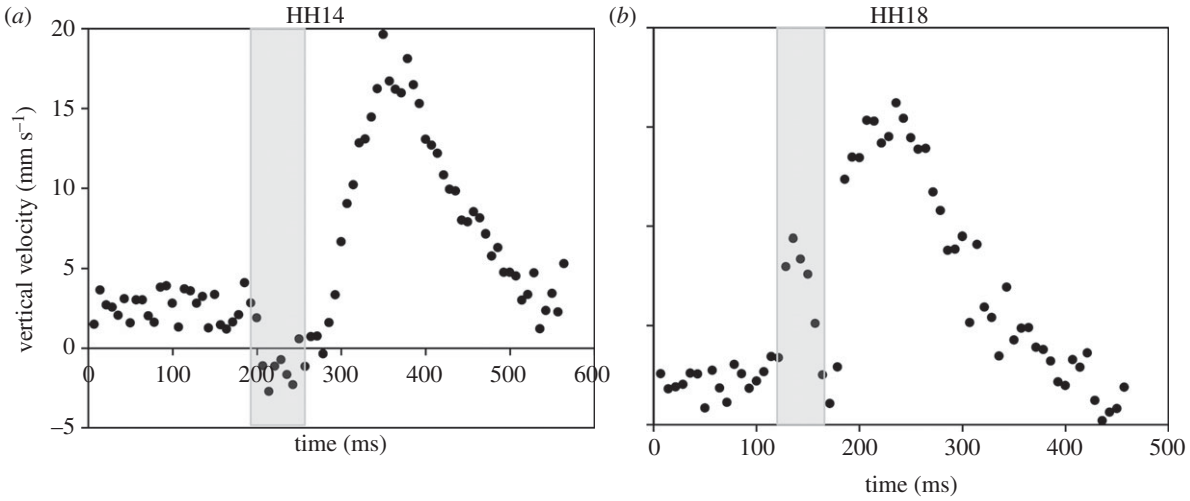

Figure 5. Velocity versus time traces of example embryos. (*a*) Vertical flow velocity at HH14 showing backflow (negative velocity, shaded) immediately prior to the systolic phase. (*b*) Velocity at HH18 showing a forward flow surge (shaded) immediately prior to the main flow during the systolic phase.

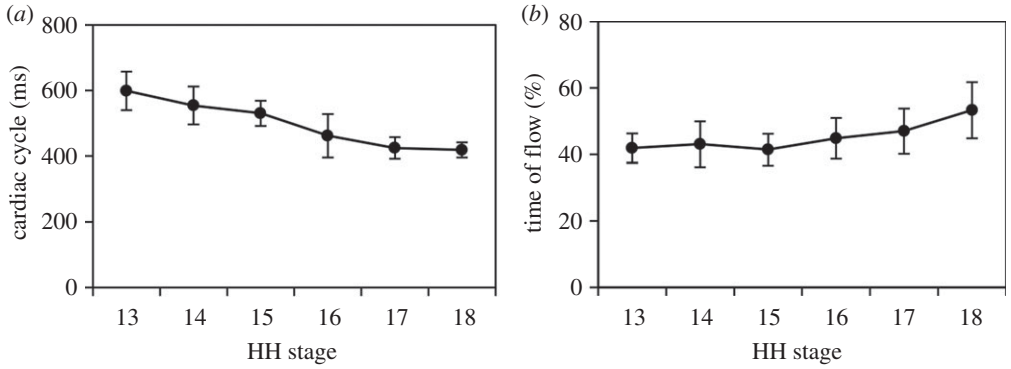

Figure 6. Summary of cardiac cycle results over advanced developmental stages from HH13 to HH18 ($n = 10$ at each stage). (*a*) Cardiac cycle (ms) and (*b*) time of flow (%). Average measures are shown at each stage with s.d.

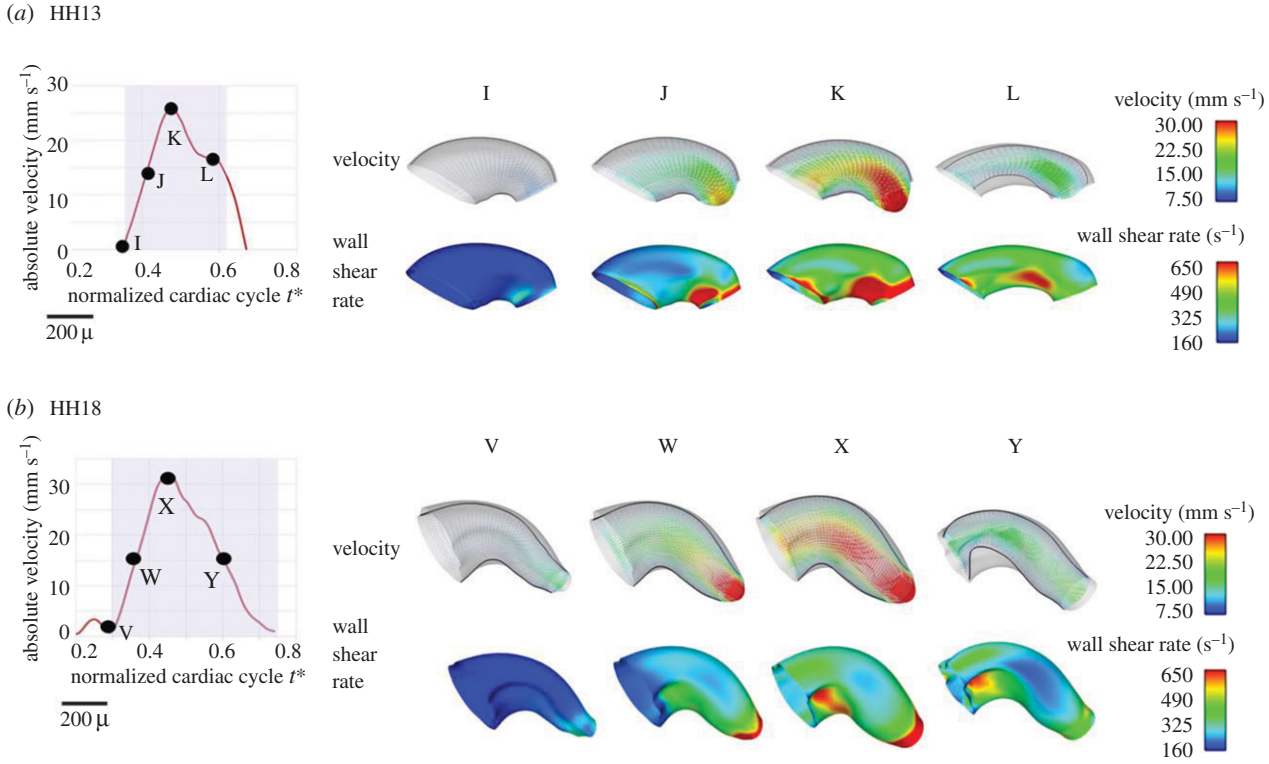

Figure 7. Embryo-specific velocity vectors and WSR distributions within the OFT from CFD models. (*a*) OFT at HH13. (*b*) OFT at HH18. For each case, a normalized cardiac cycle with representative times marked is shown. Velocity magnitudes and WSR are colour-coded.

curvatures and OFT cushions, especially in the HH18 OFT. This profile shape was expected due to centrifugal forces created by the curved geometry of the OFT. Flow velocities increased as the blood flow approached the outlet of the OFT at both HH13 and HH18 due to tapering, although centreline velocities remained higher along the whole length of the OFT at HH18. Peak WSR was attained at maximal flow conditions with the WSR being heterogeneously distributed over the OFT wall surface (figure 7*a*,*b*, bottom rows). The overall WSR remained similar (approx. 330 s^{-1}) for both HH13 and HH18 embryos; however, regions of elevated WSR (more than 900 s^{-1}) were found particularly near the OFT cushions closer to the inner curvature at both stages. Velocities and WSR results obtained from CFD modelling were consistent with experimentally obtained parameters as described above.

4. Discussion

This study characterizes the blood flow forces through the embryonic OFT during a critical developmental period, which have been shown to stimulate tissue remodelling that leads to cardiac defects [1,7,9,11,49]. Normal haemodynamic assessment is the first step in elucidating the mechanisms that cause altered blood flow to induce cardiac malformations. The intrinsic relationship between substantial changes in blood flow conditions and structural morphogenesis during cardiac looping highlights the importance of understanding the role of haemodynamics in heart formation.

The two-dimensional OCT longitudinal images acquired in this study allow for an integrated view of blood flow and OFT wall movement across a large group of embryos. Four-dimensional OCT analyses have been recently used to accurately track the dynamics of myocardial wall motion and blood flow over time [30,31,50]. While we also show four-dimensional embryo-specific CFD model examples based on four-dimensional OCT images here, four-dimensional OCT acquisition and image processing is significantly slower and more complex than two-dimensional OCT procedures and does not easily allow for routine embryo scans with large sample sizes. Instead, the variables estimated from two-dimensional longitudinal images in this study compare values at one OFT position for *peak V* and *peak Q*, and additionally for only one time point in the cardiac cycle for WSR. While simplified, the high reproducibility between samples in the same developmental stage shows our two-dimensional OCT procedure was sufficiently accurate to detect subtle changes in blood flow and structure during looping cardiac development.

The sampling location varied slightly in each stage to allow for accurate Doppler velocity measurement. Our Doppler OCT analysis requires areas of flow that are non-wrapped and non-horizontal. As the looping of the OFT and the growth of the cushions change, the geometry of the lumen from HH13 to HH18, areas of measureable blood flow change position in each developmental stage. Computational models have shown that haemodynamics vary along the length of the OFT, so that location will influence OFT diameter, blood flow velocity and wall shear stress. This study compares WSR and *D* at the time of *peak V* (and subsequent calculated measures) at each stage, since all sampling locations remained within the middle of the OFT and the small changes in positions likely have minor effects. Moreover, SV and *peak Q* should be independent of the position chosen for analysis.

4.1. Blood flow (*peak V*, *peak Q*, stroke volume and wall shear rate)

Looping and cushion generation both contribute to the geometry changes of the OFT during the HH13–HH18 development period. This cardiogenesis in turn influences the flow of blood and the resultant haemodynamic environment over the course of development. Since blood flow is expected to increase to meet the demands of the growing embryo, it is not surprising that *peak V* and *peak Q* increased from HH13 to HH18. This increase was also captured in CFD embryo-specific models of the OFT. In addition, changes in the OFT geometry influenced blood flow profiles, which were three-dimensional and skewed towards the inner curvature. The increase in blood flow velocities and flow rates in conjunction with changing curvatures of the developing OFT influenced WSR distributions obtained from the CFD models.

Overall, WSR remained relatively constant from HH13 to HH14, substantially increased from HH14 to HH15, and then steadily decreased with advanced stage reaching initial HH13 levels by HH18 (figure 4*d*). WSR was computed at the time of *peak V*, assuming a circular lumen with equation (2.4), which is a good approximation when the OFT walls are fully expanded [30,34]. The fluctuation in WSR from HH13 to HH18 was accompanied by a large increase in lumen maximum diameter between HH15 and HH18, where the initial increase in WSR preceded the increase in lumen diameter. One explanation for this response is shear-mediated vasodilation. Vasodilation is a mechanism used in other biological states, including vessel blockage, to expand the lumen and restore shear stress to normal levels [51,52]. Studies in the chick embryo have shown that the zinc finger transcription factor Krüppel-like factor 2 (KLF2) (induced by high shear stress and an activator of shear-mediated vasodilation [53]) is expressed in early embryonic endocardial cells of the OFT [54]. In their study, Groenendijk *et al.* [54] concluded that the spatial expression of KLF2 in relatively narrow portions of the embryonic heart was due to high shear stress flow. The results of our study imply that shear-induced vasodilation may play a role in normal cardiovascular development.

WSR obtained from CFD simulations depicted heterogeneous WSR distributions over the OFT lumen wall, with regions of higher WSR at OFT endocardial cushions and inner curvatures. This indicates non-uniform stimuli on the endocardial cells. Proper spatially and temporally varying WSRs may be important for the normal development of OFT endocardial cushions, which are key cardiac structures as they act as primitive valves during looping stages and later give rise to semilunar valves and a portion of the interventricular septum.

Doppler OCT analysis revealed a small volume of backflow in the OFT that decreased with advanced developmental stage. Table 2 shows that there is a transition in development where all HH14 embryos displayed backflow, while the percentage of embryos with backflow decreased as development approached HH18, at which point no embryos exhibited backflow. Additionally, an initial surge of blood flow through the OFT prior to the main flow of the cardiac cycle was evident in HH17 and HH18 embryos. This flow is in the same direction as the major flow but separated from the main surge (figure 5).

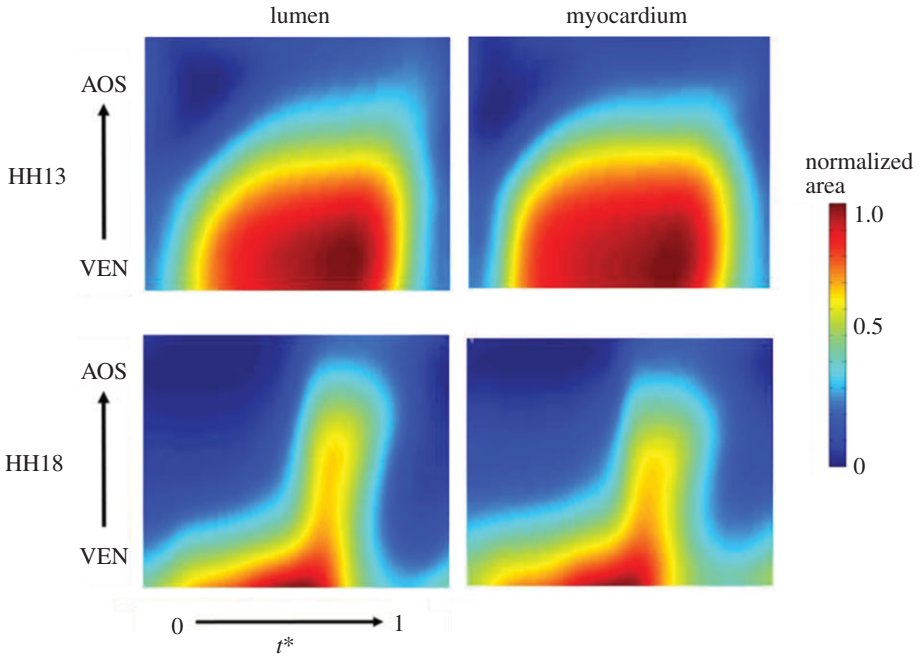

Figure 8. Changes in normalized OFT lumen and myocardium cross-sectional area over the cardiac cycle (normalized time *t**) and OFT length (normalized from ventricle, VEN, to the aortic sac, AOS).

At the earlier stages, as the ventricle fills with blood during the diastolic phase, it expands possibly exerting a suction pressure on blood flow in the OFT [55]. Endocardial cushions help to ensure unidirectional flow in the OFT by blocking the flow of blood during diastole. Backflow seen in the early stages of development between HH13 and HH17 may be caused by incomplete closure of the primitive cushions before they are fully formed. Chamber formation beginning in stages HH17–HH18 may also contribute to more efficient pumping. Additionally, backflow may decrease with advanced developmental stage because of differences in myocardial contractility between HH13 and HH18 (figure 8). While it is critical for adult heart valves to prevent intracardiac retrograde blood flow, studies in the embryonic zebrafish heart suggest that shear stimulus produced by backflow in the developing heart is required for normal valvulogenesis [56]. Our results may therefore reflect a transition in cardiac pumping that is likely essential for proper heart development.

This study thoroughly defines the relationship between SV and advanced developmental stage during looping by characterizing embryos at each stage between HH13 and HH18. This time period only spans 20 h in chick development, with short time durations between each analysis stage [12]. Increased SV throughout the progression of cardiac development reflects an increase in ventricular performance, as the heart adapts to an increased haemodynamic load. According to the Starling law, the heart can generate more force as the contractile muscle fibres stretch towards the optimal sarcomere length [57,58]. In addition, the ventricle is also developing and growing while increasing its performance. SV calculations likely overestimate actual values, since the estimation assumes that the OFT is a circular cylinder over the entire cardiac cycle. OCT images from a cross-sectional plane of the OFT show that while the myocardium concentrically contracts and expands over the cardiac cycle, the lumen is shaped like an ellipse (although almost circular) at maximum expansion and a slit at maximum contraction [30,34]. Even though this method simplifies the dynamic and complex geometry of the OFT, it does account for the changes in lumen diameter and velocity over the cardiac cycle to serve as a comparison of SV across developmental stages.

4.2. Cardiac cycle (cardiac cycle length and time of flow)

This study also analysed the timing of the cardiac cycle between HH13 and HH18 by measuring the length of the cardiac cycle and the percentage of time in the cardiac cycle with blood flow through the OFT. The cardiac cycle decreased by 1.4-fold and the time of flow remained relatively constant from HH13 to HH18. These results suggest that the interaction between cardiac cycle length, time of flow and SV are all tightly regulated in normal embryonic cardiovascular development. Using SV and cardiac cycle length to calculate cardiac output, our data show that cardiac output increases by 3.1-fold from HH13 to HH18. Despite the substantial changes in cardiac cycle and flow, the percentage of time in the cardiac cycle during which there is blood flow stays near 50% over all stages analysed.

5. Conclusion

Chicken embryos provide a valuable biological model of cardiovascular development. This is because of the developmental similarities with humans and the positioning of the embryo in the egg, which permits the implementation of a variety of *in vivo* imaging techniques (such as OCT) to measure haemodynamic conditions. The major limitation with the chicken embryo model is the lack of genetic alteration methods available to investigate the signalling mechanisms driving heart development. This study provides an important characterization of blood flow in early development that can be combined with genetic manipulation studies of cardiac formation in other animal models. Previous studies have

reported comparable haemodynamic parameters and intrinsic relationships between blood flow and cardiac development in avian, zebrafish and mammalian embryos [13,59]. For example, chick embryos and zebrafish exhibit similar ventricular growth patterns and altered blood flow in both organisms lead to impaired cardiac development. Mechanotransduction regulation of cardiac formation is only partially understood. Future work is needed in the cardiovascular development field to link changing blood flow and haemodynamics to mechanotransduction-mediated tissue remodelling. In this regard, the chicken embryo model is ideal for such studies as haemodynamic manipulations in the chick are relatively easy, while the heart is readily accessible for imaging.

Cardiac structure and ventricular performance together generate the haemodynamic environment in the embryonic OFT and play a critical role in cardiac formation. The heart undergoes significant structural changes during HH13–HH18 as the heart tube loops and forms a primitive ventricle. For reference, wet embryo weight increases by 3.8-fold between HH14 and HH18 [27]. Despite the lack of valves or autonomic innervation in early cardiac development, cardiac function including ventricular blood pressure, SV and heart rate are tightly regulated [60], as cardiac output increases proportionally to embryo weight [27]. This study used an integrative imaging and modelling approach to characterize the relationship between form and function of the developing heart in order to improve understanding of the processes involved in the development of the cardiovascular system. This new knowledge quantifies normal patterns of haemodynamic change in the early cardiac looping stages, which will be fundamental to future investigations of altered biomechanical environments that lead to cardiac defects.

Data accessibility. The datasets supporting this article have been uploaded as part of the electronic supplementary material.

Authors' contributions. M.M. coordinated the study, carried out a large portion of the data collection and data analysis, and drafted the manuscript; V.C. carried out all of the CFD modelling and analysis, and contributed to the manuscript; C.D. and S.W. collected preliminary data and participated in data analysis; S.R. conceived of the study and helped draft the manuscript.

Competing interests. We declare we have no competing interests.

Funding. This work has been supported by grant NIH R01 HL094570 to S.R.; by a Charles Patrick Memorial scholarship to M.M., and Pete and Rosalie Johnson Scholarships to C.D. and S.W. The content is solely the responsibility of the authors and does not necessarily represent the official views of grant-giving bodies.

References

1. Sedmera D, Pexieder T, Rychterova V, Hu N, Clark EB. 1999 Remodeling of chick embryonic ventricular myoarchitecture under experimentally changed loading conditions. *Anat. Rec.* **254**, 238–252. (doi:10.1002/(SICI)1097-0185(19990201)254:2<238::AID-AR10>3.0.CO;2-V)
2. Sedmera D, Thompson RP. 2011 Myocyte proliferation in the developing heart. *Dev. Dyn.* **240**, 1322–1334. (doi:10.1002/dvdy.22650)
3. Hove JR, Koster RW, Forouhar AS, Acevedo-Bolton G, Fraser SE, Gharib M. 2003 Intracardiac fluid forces are an essential epigenetic factor for embryonic cardiogenesis. *Nature* **421**, 172–177. (doi:10.1038/nature01282)
4. Fisher AB, Chien S, Barakat AI, Nerem RM. 2001 Endothelial cellular response to altered shear stress. *Am. J. Physiol. Lung Cell. Mol. Physiol.* **281**, L529–L533.
5. Van der Heiden K, Groenendijk BC, Hierck BP, Hogers B, Koerten HK, Mommaas AM, Gittenberger-de Groot AC, Poelmann RE. 2006 Monocilia on chicken embryonic endocardium in low shear stress areas. *Dev. Dyn.* **235**, 19–28. (doi:10.1002/dvdy.20557)
6. Davies PF. 1995 Flow-mediated endothelial mechanotransduction. *Physiol. Rev.* **75**, 519–560.
7. Clark EB, Rosenquist GC. 1978 Spectrum of cardiovascular anomalies following cardiac loop constriction in the chick embryo. *Birth Defects Orig. Artic. Ser.* **14**, 431–442.
8. Gittenberger-de Groot AC, Bartelings MM, Deruiter MC, Poelmann RE. 2005 Basics of cardiac development for the understanding of congenital heart malformations. *Pediatr. Res.* **57**, 169–176. (doi:10.1203/01.pdr.0000148710.69159.61)
9. Hogers B, DeRuiter MC, Gittenberger-de Groot AC, Poelmann RE. 1997 Unilateral vitelline vein ligation alters intracardiac blood flow patterns and morphogenesis in the chick embryo. *Circ. Res.* **80**, 473–481. (doi:10.1161/01.RES.80.4.473)
10. Reckova M, Rosengarten C, deAlmeida A, Stanley CP, Wessels A, Gourdie RG, Thompson RP, Sedmera D. 2003 Haemodynamics is a key epigenetic factor in development of the cardiac conduction system. *Circ. Res.* **93**, 77–85. (doi:10.1161/01.res.0000079488.91342.b7)
11. Tobita K, Schroder EA, Tinney JP, Garrison JB, Keller BB. 2002 Regional passive ventricular stress–strain relations during development of altered loads in chick embryo. *Am. J. Physiol. Heart Circ. Physiol.* **282**, H2386–H2396. (doi:10.1152/ajpheart.00879.2001)
12. Hamburger V, Hamilton HL. 1951 A series of normal stages in the development of the chick embryo. *Dev. Dyn.* **195**, 231–272. (doi:10.1002/aja.1001950404)
13. Goenezen S, Rennie MY, Rugonyi S. 2012 Biomechanics of early cardiac development. *Biomech. Modell. Mechanobiol.* **11**, 1187–1204. (doi:10.1007/s10237-012-0414-7)
14. Taber LA. 1998 Mechanical aspects of cardiac development. *Prog. Biophys. Mol. Biol.* **69**, 237–255. (doi:10.1016/S0079-6107(98)00010-8)
15. Baker K, Holtzman NG, Burdine RD. 2008 Direct and indirect roles for nodal signaling in two axis conversions during asymmetric morphogenesis of the zebrafish heart. *Proc. Natl Acad. Sci. USA* **105**, 13 924–13 929. (doi:10.1073/pnas.0802159105)
16. Mercola M, Levin M. 2001 Left–right asymmetry determination in vertebrates. *Annu. Rev. Cell Dev. Biol.* **17**, 779–805. (doi:10.1146/annurev.cellbio.17.1.779)
17. Taber LA, Lin IE, Clark EB. 1995 Mechanics of cardiac looping. *Dev. Dyn.* **203**, 42–50. (doi:10.1002/aja.1002030105)
18. Patten BM. 1922 The formation of the cardiac loop in the chick. *Am. J. Anat.* **30**, 373–397. (doi:10.1002/aja.1000300304)
19. Stalsberg H. 1969 Regional mitotic activity in the precardiac mesoderm and differentiating heart tube in the chick embryo. *Dev. Biol.* **20**, 18–45. (doi:10.1016/0012-1606(69)90003-7)
20. Itasaki N, Nakamura H, Sumida H, Yasuda M. 1991 Actin bundles on the right side in the caudal part of the heart tube play a role in dextro-looping in the embryonic chick heart. *Anat. Embryol.* **183**, 29–39. (doi:10.1007/BF00185832)
21. Taber LA, Hu N, Pexieder T, Clark EB, Keller BB. 1993 Residual strain in the ventricle of the stage 16–24 chick embryo. *Circulation research*. **72**, 455–462. (doi:10.1161/01.RES.72.2.455)
22. Broekhuizen ML, Hogers B, DeRuiter MC, Poelmann RE, Gittenberger-de Groot AC, Wladimiroff JW. 1999 Altered hemodynamics in chick embryos after extraembryonic venous obstruction. *Ultrasound Obstet. Gynecol.* **13**, 437–445. (doi:10.1046/j.1469-0705.1999.13060437.x)
23. Hogers B, DeRuiter MC, Gittenberger-de Groot AC, Poelmann RE. 1999 Extraembryonic venous obstructions lead to cardiovascular malformations and can be embryolethal. *Cardiovasc. Res.* **41**, 87–99. (doi:10.1016/S0008-6363(98)00218-1)
24. Ursem NT, Stekelenburg-de Vos S, Wladimiroff JW, Poelmann RE, Gittenberger-de Groot AC, Hu N, Clark EB. 2004 Ventricular diastolic filling characteristics in

stage-24 chick embryos after extra-embryonic venous obstruction. *J. Exp. Biol*. **207**, 1487–1490. (doi:10.1242/jeb.00902)

25. Keller BB, Hu N, Clark EB. 1990 Correlation of ventricular area, perimeter, and conotruncal diameter with ventricular mass and function in the chick embryo from stages 12 to 24. *Circ. Res*. **66**, 109–114. (doi:10.1161/01.RES.66.1.109)
26. Faber JJ, Green TJ, Thornburg KL. 1974 Embryonic stroke volume and cardiac output in the chick. *Dev. Biol*. **41**, 14–21. (doi:10.1016/0012-1606(74)90278-4)
27. Hu N, Clark EB. 1989 Haemodynamics of the stage 12 to stage 29 chick embryo. *Circ. Res*. **65**, 1665–1670. (doi:10.1161/01.RES.65.6.1665)
28. Hu N, Connuck DM, Keller BB, Clark EB. 1991 Diastolic filling characteristics in the stage 12 to 27 chick embryo ventricle. *Pediatr. Res*. **29**, 334–337. (doi:10.1203/00006450-199104000-00002)
29. Hu N, Keller BB. 1995 Relationship of simultaneous atrial and ventricular pressures in stage 16–27 chick embryos. *Am. J. Physiol*. **269**, H1359–H1362.
30. Liu A, Yin X, Shi L, Li P, Thornburg KL, Wang R, Rugonyi S. 2012 Biomechanics of the chick embryonic heart outflow tract at HH18 using 4D optical coherence tomography imaging and computational modeling. *PLoS ONE* **7**, e40869. (doi:10.1371/journal.pone.0040869)
31. Ma Z, Liu A, Yin X, Troyer A, Thornburg K, Wang RK, Rugonyi S. 2010 Measurement of absolute blood flow velocity in outflow tract of HH18 chicken embryo based on 4D reconstruction using spectral domain optical coherence tomography. *Biomed. Opt. Expr*. **1**, 798–811. (doi:10.1364/boe.1.000798)
32. Shi L, Goenezen S, Haller S, Hinds MT, Thornburg KL, Rugonyi S. 2013 Alterations in pulse wave propagation reflect the degree of outflow tract banding in HH18 chicken embryos. *Am. J. Physiol. Heart Circ. Physiol*. **305**, H386–H396. (doi:10.1152/ajpheart.00100.2013)
33. Midgett M, Goenezen S, Rugonyi S. 2014 Blood flow dynamics reflect degree of outflow tract banding in Hamburger–Hamilton stage 18 chicken embryos. *J. R. Soc. Interface*. **11**, 20140643. (doi:10.1098/rsif.2014.0643)
34. Manner J, Thrane L, Norozi K, Yelbuz TM. 2008 High-resolution *in vivo* imaging of the cross-sectional deformations of contracting embryonic heart loops using optical coherence tomography. *Dev. Dyn.* **237**, 953–961. (doi:10.1002/dvdy.21483)
35. Liu A, Wang R, Thornburg KL, Rugonyi S. 2009 Efficient postacquisition synchronization of 4-D nongated cardiac images obtained from optical coherence tomography: application to 4-D reconstruction of the chick embryonic heart. *J. Biomed. Opt*. **14**, 044020. (doi:10.1117/1.3184462)
36. Yin X, Liu A, Thornburg KL, Wang RK, Rugonyi S. 2012 Extracting cardiac shapes and motion of the chick embryo heart outflow tract from four-dimensional optical coherence tomography images. *J. Biomed. Opt*. **17**, 96005-1. (doi:10.1117/1.jbo.17.9.096005)
37. Liu A, Nickerson A, Troyer A, Yin X, Cary R, Thornburg K, Wang R, Rugonyi S. 2011 Quantifying blood flow and wall shear stresses in the outflow tract of chick embryonic hearts. *Comput. Struct*. **89**, 855–867. (doi:10.1016/j.compstruc.2011.03.003)
38. Rugonyi S, Shaut C, Liu A, Thornburg K, Wang RK. 2008 Changes in wall motion and blood flow in the outflow tract of chick embryonic hearts observed with optical coherence tomography after outflow tract banding and vitelline-vein ligation. *Phys. Med. Biol*. **53**, 5077–5091. (doi:10.1088/0031-9155/53/18/015)
39. Nicholas WW, O'Rourke MF, Vlachopoulos C. 2011 *McDonald's blood flow in arteries: theoretical, experimental, and clinical principles*. London, UK: Hodder and Arnold.
40. Phoon CK, Aristizabal O, Turnbull DH. 2002 Spatial velocity profile in mouse embryonic aorta and Doppler-derived volumetric flow: a preliminary model. *Am. J. Physiol. Heart Circ. Physiol*. **283**, H908–H916. (doi:10.1152/ajpheart.00869.2001)
41. Katritsis D, Kaiktsis L, Chaniotis A, Pantos J, Efstathopoulos EP, Marmarelis V. 2007 Wall shear stress: theoretical considerations and methods of measurement. *Prog. Cardiovasc. Dis*. **49**, 307–329. (doi:10.1016/j.pcad.2006.11.001)
42. Welty J, Wicks CE, Rorrer GL, Wilson RE. 2008 *Fundamentals of momentum, heat and mass transfer*. Hoboken, NJ: John Wiley and Sons, Inc.
43. Al-Roubaie S, Jahnsen ED, Mohammed M, Henderson-Toth C, Jones EA. 2011 Rheology of embryonic avian blood. *Am. J. Physiol. Heart Circ. Physiol*. **301**, H2473–H2481. (doi:10.1152/ajpheart.00475.2011)
44. Butcher JT, McQuinn TC, Sedmera D, Turner D, Markwald RR. 2007 Transitions in early embryonic atrioventricular valvular function correspond with changes in cushion biomechanics that are predictable by tissue composition. *Circ. Res*. **100**, 1503–1511. (doi:10.1161/circresaha.107.148684)
45. Goenezen S, Chivukula VK, Midgett M, Phan L, Rugonyi S. 2015 4D subject-specific inverse modeling of the chick embryonic heart outflow tract hemodynamics. *Biomech. Model. Mechanobiol*., 1–21. (doi:10.1007/s10237-015-0720-y)
46. Vennemann P *et al.* 2006 *In vivo* micro particle image velocimetry measurements of blood-plasma in the embryonic avian heart. *J. Biomech*. **39**, 1191–1200. (doi:10.1016/j.jbiomech.2005.03.015)
47. Poelma C, Van der Heiden K, Hierck BP, Poelmann RE, Westerweel J. 2010 Measurements of the wall shear stress distribution in the outflow tract of an embryonic chicken heart. *J. R. Soc. Interface*. **7**, 91–103. (doi:10.1098/rsif.2009.0063)
48. Oosterbaan AM, Ursem NT, Struijk PC, Bosch JG, van der Steen AF, Steegers EA. 2009 Doppler flow velocity waveforms in the embryonic chicken heart at developmental stages corresponding to 5–8 weeks of human gestation. *Ultrasound Obstet. Gynecol.* **33**, 638–644. (doi:10.1002/uog.6362)
49. Clark EB, Hu N, Frommelt P, Vandekieft GK, Dummett JL, Tomanek RJ. 1989 Effect of increased pressure on ventricular growth in stage 21 chick embryos. *Am. J. Physiol. Heart Circ. Physiol*. **257**, H55–H61.
50. Happel CM, Thommes J, Thrane L, Manner J, Ortmaier T, Heimann B, Yelbuz TM. 2011 Rotationally acquired four-dimensional optical coherence tomography of embryonic chick hearts using retrospective gating on the common central A-scan. *J. Biomed. Opt*. **16**, 096007. (doi:10.1117/1.3622491)
51. Koller A, Kaley G. 1989 Flow velocity-dependent regulation of microvascular resistance *in vivo*. *Microcirc. Endothelium Lymphatics* **5**, 519–529.
52. Castier Y, Brandes RP, Leseche G, Tedgui A, Lehoux S. 2005 p47phox-dependent NADPH oxidase regulates flow-induced vascular remodeling. *Circ. Res*. **97**, 533–540. (doi:10.1161/01.res.0000181759.63239.21)
53. Dekker RJ, van Soest S, Fontijn RD, Salamanca S, de Groot PG, VanBavel E, Pannekoek H, Horrevoets AJ. 2002 Prolonged fluid shear stress induces a distinct set of endothelial cell genes, most specifically lung Krüppel-like factor (KLF2). *Blood* **100**, 1689–1698. (doi:10.1182/blood-2002-01-0046)
54. Groenendijk BC, Hierck BP, Gittenberger-De Groot AC, Poelmann RE. 2004 Development-related changes in the expression of shear stress responsive genes KLF-2, ET-1, and NOS-3 in the developing cardiovascular system of chicken embryos. *Dev. Dyn.* **230**, 57–68. (doi:10.1002/dvdy.20029)
55. Phelan CM, Hughes SF, Benson DWJr. 1995 Heart rate-dependent characteristics of diastolic ventricular filling in the developing chick embryo. *Pediatr. Res*. **37**, 289–293. (doi:10.1203/00006450-199503000-00007)
56. Vermot J, Forouhar AS, Liebling M, Wu D, Plummer D, Gharib M, Fraser SE. 2009 Reversing blood flows act through *klf2a* to ensure normal valvulogenesis in the developing heart. *PLoS Biol*. **7**, e1000246. (doi:10.1371/journal.pbio.1000246)
57. Gordon AM, Huxley AF, Julian FJ. 1966 The variation in isometric tension with sarcomere length in vertebrate muscle fibres. *J. Physiol*. **184**, 170–192. (doi:10.1113/jphysiol.1966.sp007909)
58. Ramsey RW, Street SF. 1940 The isometric length–tension diagram of isolated skeletal muscle fibers of the frog. *J. Cell Comp. Physiol*. **15**, 11–34. (doi:10.1002/jcp.1030150103)
59. Furst B. 2014 *Haemodynamics of the early embryo circulation*, 21–9. London, UK: Springer.
60. Clark EB, Hu N, Dummett JL, Vandekieft GK, Olson C, Tomanek R. 1986 Ventricular function, morphology in chick embryo from stages 18 to 29. *Am. J. Physiol*. **250**, H407–H413.